SAR COMPLIANCE TESTING OF FUJITSU MODEL EC2500 CELLULAR TELEPHONE

FINAL TECHNICAL REPORT

November 23, 1998

Submitted to:

Mr. Tom Tidwell
KTL Dallas, Inc.
802 N. Kealy Street
Lewisville, TX 75057-3136

Submitted by:

Om P. Gandhi
Professor and Chairman
University of Utah
Electrical Engineering Department
50 S Central Campus Dr., Rm. 3280
Salt Lake City, UT 84112 9206

SAR COMPLIANCE TESTING OF FUJITSU MODEL EC2500
CELLULAR TELEPHONE

I. Introduction

The U.S. Federal Communications Commission (FCC) has adopted limits of human exposure to RF emissions from mobile and portable devices that are regulated by the FCC [1]. The FCC has also recently issued Supplement C (Edition 97 01) to OET Bulletin 65 defining both the measurement and the computational procedures that should be followed for evaluating compliance of mobile and portable devices with FCC limits for human exposure to radiofrequency emissions [2].

For the Fujitsu Model EC2500 Cellular Telephone, we have used the experimental measurement techniques to determine the SAR distributions from which the peak 1-g SARs are obtained at low band (channel 1013, frequency = 824.70 MHz), the midband (channel 383, frequency = 836.49 MHz) and at the high end (channel 799, frequency = 848.97 MHz), respectively. Furthermore, since this telephone has a retractable antenna, the SAR distributions were measured both for the antenna pulled out or left retracted for each of the three bands, respectively. As recommended in [2], the telephone was placed against the left ear with the antenna located towards the front of the head. This allows the antenna to be in close proximity to the model of the head resulting in higher SARs allowing, thereby, the worst case determination of absorbed energy in the user's head [3]. Also as recommended in [2], the SAR distributions were measured without the model of a hand to determine the worst case SARs.

II. The Fujitsu Model EC2500 Cellular Telephone

The Fujitsu Model EC2500 Cellular Telephone (FCC ID# CFD825FBCP 201) operates in the frequency band 824.7-848.97 MHz. It is capable of operating as a dual mode telephone with the analog mode allowing transmitted powers as high as 28.0 dBm (631 mW) and the digital CDMA mode radiating powers typically on the order of 23 dBm

(200 mW). A coaxial output port is provided at the back of the telephone which may be used to measure the power output of the power amplifier by using a coaxial cable of measured insertion loss 0.5 dB. By using a Hewlett Packard (HP) Model 436A Power Meter with HP Model 8481 Power Sensor, we measured the power output of the Fujitsu Model EC2500 Cellular Telephone at the low frequency end (channel 1013, 824.70 MHz), at midband (channel 383, 836.49 MHz) and at the high end (channel 799, 848.97 MHz), respectively. After correcting for the coaxial cable loss of 0.5 dB, the measured output powers for this Fujitsu Model EC2500 Cellular Telephone operating at the CDMA digital mode (higher power setting) are given in Table 1.

The telephone uses a monopole antenna which can either be pulled out or left retracted. As recommended in [2], the SAR distributions were, therefore, measured for this telephone both for the antenna pulled out or left retracted for the low end frequency (channel 1013, 824.70 MHz), at a midband frequency (channel 383, 836.49 MHz) and at a high end frequency (channel 799, 848.97 MHz). Also, since the higher power setting for the digital CDMA mode produces considerably higher power outputs, the telephone was tested for each of these frequencies for this setting of the telephone. A photograph of the Fujitsu Model EC2500 Cellular Telephone is given in Fig. 1.

III. The Tissue-Simulant Model

For measurements of SAR distributions, we have used the Utah Experimental Model that is described in detail in [4]. This model uses a lossy outer shell of the following approximate dimensions:

Axial length from chin to top of the head = 26 cm
Distance from location of the ear canal to top of the head = 14.7 cm
Width from side to side = 16.5 cm

These dimensions are typical for adult human beings. The shell thickness of the head and neck model is approximately 4–7 mm, which is typical of the human skull

thickness. The thickness for the ear region is, however, considerably less and is only about 3 mm.

This experimental model shown in Fig. 2 has, in the past, been used for comparison of the measured peak 1 g SARs with those obtained with the Utah FDTD Code for ten wireless telephones, five at 835 MHz and five for PCS (1900 MHz) frequencies [see Table 2]. The numerical SARs were obtained using the anatomically-based, 15-tissue Utah model of the head and neck with a resolution of 1.974 × 1.974 × 3.0 mm that has been described in the scientific literature through numerous publications (see e.g. references 3, 5). The measured and calculated 1-g SARs for these ten telephones, including some research test samples from diverse manufacturers using a variety of radiating antennas for different source-based time-averaged powers are compared in Table 2 [4]. Even though widely different peak 1 g SARs from 0.13 to 5.41 W/kg are obtained because of the variety of antennas and handsets, agreement between the calculated and the measured data is excellent and generally within ± 25 percent.

These tests validate the Utah Experimental Phantom Model as being capable of giving peak 1 g SARs that are in good agreement with the SARs obtained with the realistic, anatomically-based model of the human head and neck both at 835 and 1900 MHz.

The head and neck and the upper part of the torso of the model are filled with a liquid with measured electrical properties (dielectric constant and conductivity) close to the average properties of the brain for white and gray matters in the frequency band 824 849 MHz. This corresponds to $\varepsilon_r = 43.5$ and $\sigma = 0.9$ S/m. For a composition of 40.4% water, 56.0% sugar, 2.5% salt (NaCℓ) and 1.0% HEC, we have measured the values of $\varepsilon_r = 41.1 \pm 1.4$ and $\sigma = 1.06 \pm 0.05$ S/m at the center band frequency of 835 MHz using the HP Model 85070 B Dielectric Probe in conjunction with HP Model 8720 C Network Analyzer (50 MHz - 20 GHz). Since these values are very close to the desired values for ε_r and σ, this composition was, therefore, used as the biological phantom material to fill the model shown in Fig. 2.

The SAR distributions were measured using the automated 3-D stepper-motor driven SAR measurement system described in [4]. To the extent that the conductivity σ is slightly higher and the permittivity ε_r is somewhat lower than the desired values, it should help in avoiding underestimating the SAR [2].

IV. The E-Field Probe

The non-perturbing implantable E-field probe used in the setup was originally developed by Bassen et al. [6] and is now manufactured by L3/Narda Microwave Corporation, Hauppauge, New York as Model 8021 E-field probe. In this probe, three orthogonal miniature dipoles are placed on a triangular beam substrate. Each dipole is loaded with a small Schottky diode and connected to the external circuitry by high resistance (2 MΩ ± 40%) leads to reduce secondary pickups. The entire structure is then encapsulated with a low dielectric constant insulating material. The probe thus constructed has a very small (4 mm) diameter, which results in a relatively small perturbation of the internal electric field.

Test for Square Law Region

It is necessary to operate the E-field probe in the square law region for each of the diodes so that the sum of the dc voltage outputs from the three dipoles is proportional to the square of the internal electric field ($|E_i|^2$). Fortunately, the personal wireless devices induce SARs that are generally less than 5-6 W/kg even for closest locations of the head [3]. For compliance testing, it is, therefore, necessary that the E-field probe be checked for square law behavior for SARs up to such values that are likely to be encountered. Such a test may be conducted using a canonical lossy body such as a rectangular box or a sphere irradiated by a dipole. By varying the radiated power of the dipole, the output of the probe should increase linearly with the applied power for each of the test locations.

Shown in Figs. 3a, 3b are the results of the tests performed to check the square law behavior of the E-field probe used in our setup at 840 and 1900 MHz, respectively. For

these measurements, we have used a rectangular box of dimensions 30 × 15 × 50 cm that was irradiated by the corresponding half wave dipoles with different amounts of radiated powers from 200-800 mW. Since the dc voltage outputs of the probe are fairly similar when normalized to a radiated power of 100 mW, the square law behavior is demonstrated and an output voltage that is proportional to $|E_i|^2$ is obtained within ± 3 percent.

Test for Isotropy of the Probe

Another important characteristic of the probe that affects the measurement accuracy is its isotropy. Since the orientation of the induced electric field is generally unknown, the E-field probe should be relatively isotropic in its response to the orientation of the E-field. Shown in Figs. 4a, 4b are the test results of the E-field probe used in our setup at 840 and 1900 MHz, respectively. The previously described box phantom of dimensions 30 × 15 × 50 cm along x, y and z dimensions, respectively, was also used for these measurements. This phantom was filled to a depth of 15 cm with a tissue-simulant fluid of composition given in Section III. The E-field probe was rotated around its axis from 0 to 360° in incremental steps of 60°. An isotropy of less than ± 0.23 dB (± 5.5%) was observed for this E-field probe both at 840 and 1900 MHz.

Calibration of the E-Field Probe

Since the voltage output of the E-field probe is proportional to the square of the internal electric field ($|E_i|^2$), the SAR, given by $\sigma|E_i|^2/\rho$ is, therefore, proportional to the voltage output of the E-field probe by a proportionality constant C. The constant C is defined as the calibration factor, and is frequency and material dependent. It is measured to calibrate the probe at the various frequencies of interest using the appropriate tissue-simulating materials for the respective frequencies.

Canonical geometries such as waveguides, rectangular slabs and layered or homogeneous spheres have, in the past, been used for the calibration of the implantable E-field probe [7-9]. Since the Finite Difference Time Domain (FDTD) has been carefully validated to solve electromagnetic problems for a variety of geometries [8, 10], we were

able to calibrate the Narda E-field probe by comparing the measured variations of the probe voltage ($\approx |E_i|^2$) against the FDTD-calculated variations of SARs for a box phantom of dimensions 30 × 15 × 50 cm used previously for the data given in Figs. 3a, b, respectively. For these measurements, we placed the nominal half wave dipoles of lengths 178 mm and 77 mm at 840 and 1900 MHz, respectively, at several distances d (see inserts of Figs. 5a, 5b, and 6a, 6b) from the outer surface of the acrylic (ε_r = 2.56) box of thickness 6.55 mm. Shown in Figs. 5a, 5b and 6a, 6b are the comparisons between the experimentally measured and FDTD calculated variations of the SAR distributions for this box phantom. Since there are excellent agreements between the calculated SARs and the measured variations of the voltage output of the E field probe for four different separations d of the half wave dipoles at each of the two frequencies, it is possible to calculate the calibration factors at the respective frequencies. For the Narda Model 8021 E-field probe used in our setup, the calibration factors are determined to be 0.49 and 0.84 (mW/kg)/μV at 840 and 1900 MHz, respectively.

V. Experimental Results: Canonical Problems

To further validate the system, it has been used to measure the peak 1-g SAR for the above-mentioned box phantom and a glass sphere model of thickness 5 mm, external diameter = 223 mm and assumed dielectric constant ε_r = 4.0. This sphere model is once again filled with the corresponding brain simulant fluids. Shown in Figs. 7a, 7b and 8a, 8b are the measured and FDTD-calculated SAR distributions inside the sphere for various separations d between the dipole and the sphere (see insert for Figs. 7, 8). Comparison of the measured and FDTD-calculated peak 1-g SARs for both phantom geometries are given in Tables 3 and 4, respectively. As can be seen, the agreement between experimental measurement and numerical simulation is excellent and generally within ± 10 percent for both rectangular and spherical phantoms.

VI. Measurement Uncertainty: Test Runs With Cellular Telephones

The automated setup shown in Fig. 2 has been used for the testing of ten personal wireless devices including some research test samples, five each at 835 and 1900 MHz, respectively [4]. Given in Table 2 is the comparison of the numerical and measured peak 1-g SARs for these devices using our experimental phantom model and the FDTD-based numerical procedure used for calculations of SAR distributions for an anatomically-based model of the head of an adult male [4]. The measured and calculated SARs for the ten telephones which have quite different operational modes (TDMA, CDMA, etc.) and antenna structures (helical, monopole, or helix-monopole) vary from 0.13 to 5.41 W/kg. Even though widely different peak 1 g SARs are obtained because of the variety of antennas and handsets, agreement between the calculated and the measured data is excellent and generally within ± 25%. This is particularly remarkable since an MRI-derived, 16-tissue anatomically-based model of the adult human head is used for FDTD calculations and a relatively simplistic two tissue phantom model is used for experimental peak 1-g SAR measurements.

We estimate the uncertainty of our measuring system to be ± 12.5 percent. As seen in Table 2, an agreement within ± 25 percent is obtained for the peak 1-g SARs calculated using the Utah FDTD Code and the Utah Experimental Phantom Model for ten assorted wireless devices using a variety of antennas and handset dimensions. Since both the numerical and experimental methods are completely independent methods, and each is prone to its own set of errors, an uncertainty of ± 12.5 percent can be ascribed to each of the methods.

VII. The Measured SAR Distributions for Fujitsu Model EC2500 Cellular Telephone

As suggested in Supplement C (Edition 97-01) to the FCC OET Bulletin 65 [2], the SAR measurements have been conducted with the Fujitsu Model EC2500 Cellular Telephone pressed against the model of the head such that the center of the ear piece is

aligned against the location of the ear canal. Furthermore, the handset is oriented such that the center line of the body of the handset is in the plane passing through the two ear canals and the tip of the mouth.

The highest SAR regions for each of the frequencies and antenna configurations (pulled out or left retracted) were determined in the first instance by using coarser sampling with a step size of 8.0 mm over three overlapping scan areas for a total scan area of 8.0 × 9.6 cm. After identifying the regions of the highest SAR for each of the six cases (three frequencies and two antenna configurations for each of these frequencies), the SAR distributions were measured with a resolution of 2 mm in order to obtain the peak 1 cm^3 or 1-g SAR.

The measured SAR distributions normalized to the maximum planned radiated power of 28.0 dBm (631 mW) are given in Tables 5 10, respectively. The peak 1-g SARs thus determined are given in Table 11. All of the measured peak 1-g SARs are less than 1.0 W/kg and are, therefore, lower than the peak 1 g SAR of 1.6 W/kg suggested in the FCC 96-326 Guidelines [1].

VIII. Comparison of the Data With FCC 96-326 Guidelines

According to the FCC 96-326 Guidelines [1], the peak SAR for any 1-g of tissue should not exceed 1.6 W/kg. For a maximum radiated power of 28.0 dBm (631 mW), we have determined the peak 1-g SARs for the Fujitsu Model EC2500 Cellular Telephone to be less than 1.0 W/kg. This is lower than 1.6 W/kg suggested in the FCC 96-326 Guidelines [1].

REFERENCES

1. Federal Communications Commission, "Guidelines for Evaluating the Environmental Effects of Radiofrequency Radiation," FCC 96-326, August 1, 1996.

2. K. Chan, R. F. Cleveland, Jr., and D. L. Means, "Evaluating Compliance With FCC Guidelines for Human Exposure to Radiofrequency Electromagnetic Fields," Supplement C (Edition 97-01) to OET Bulletin 65, December, 1997. Available from Office of Engineering and Technology, Federal Communications Commission, Washington D.C., 20554.

3. O. P. Gandhi, G. Lazzi and C. M. Furse, "Electromagnetic Absorption in the Human Head and Neck for Mobile Telephones at 835 and 1900 MHz," *IEEE Transactions on Microwave Theory and Techniques*, Vol. 44, pp. 1884 1897, 1996.

4. Q. Yu, O. P. Gandhi, M. Aronsson, and D. Wu, "An Automated SAR Measurement System for Compliance Testing of Personal Wireless Devices," *IEEE Transactions on Electromagnetic Compatibility*, Vol. 41(3), pp. 234-245, August 1999.

5. O. P. Gandhi, "FDTD in Bioelectromagnetics: Safety Assessment and Medical Applications," Chapter 11, pp. 613-651 in *Advances in Computational Electrodynamics: The FDTD Method*, edited by A. Taflove, Artech House Inc., Dedham, MA, 1998.

6. H. I. Bassen and G. S. Smith, "Electric Field Probes -- A Review," *IEEE Trans. Antennas Propagation*, Vol. 34, pp. 710-718, September 1983.

7. D. Hill, "Waveguide Techniques for the Calibration of Miniature Electric Field Probes for Use in Microwave Bioeffects Studies," *IEEE Trans. Microwave Theory Tech.*, Vol. 30, pp. 92-94, 1982.

8. N. Kuster and Q. Balzano, "Energy Absorption Mechanism by Biological Bodies in the Near Field of Dipole Antennas Above 300 MHz," *IEEE Trans. Veh. Technology*, Vol. 41, pp. 17-23, 1992.

9. M. A. Stuchly, S. S. Stuchly, and A. Kraszewski, "Implantable Electric Field Probes -- Some Performance Characteristics," *IEEE Trans. Biomed. Eng.*, Vol. 31, pp. 526-531, 1984.

10. C. M. Furse, Q. Yu, and O. P. Gandhi, "Validation of the Finite-Difference Time-Domain Method for Near-Field Bioelectromagnetic Simulations," *Microwave and Optical Technology Letters*, Vol. 16, pp. 341 345, 1997.

Table 1. The measured time-averaged conducted power of the Fujitsu Model EC2500 Cellular Telephone.

Channel #	Frequency MHz	Measured Power Output mW
1013 Low end	824.70	627 (27.97 dBm)
383 Midband	836.49	625 (27.96 dBm)
799 High end	848.97	621 (27.93 dBm)

Table 2. Comparison of the experimentally measured and FDTD-calculated peak 1-g SARs for ten wireless telephones, five each at 835 and 1900 MHz, respectively.

	Time-Averaged Radiated Power mW	Using Experimental Model W/kg	Numerical Method W/kg
Cellular Telephones at 835 MHz			
Telephone A	600	4.02	3.90
Telephone B	600	5.41	4.55
Telephone C	600	4.48	3.52
Telephone D	600	3.21	2.80
Telephone E	600	0.54	0.53
PCS Telephones at 1900 MHz			
Telephone A	125	1.48	1.47
Telephone B	125	0.13	0.15
Telephone C	125	0.65	0.81
Telephone D	125	1.32	1.56
Telephone E	99.3	1.41	1.25

Table 3. Box phantom: Comparison of the measured and FDTD-calculated peak 1-g SARs for four spacings each at 840 and 1900 MHz, radiated power normalized to 0.5 W.

Frequency (MHz)	Distance (mm) Between λ/2 Dipole and the Box	SAR (W/kg)		Difference (%)
		Measured	FDTD	
840	17.5	4.58	4.20	+8.3
840	22.5	3.53	3.65	-3.4
840	27.5	2.69	3.00	-10.2
840	33.0	1.95	2.24	-12.9
1900	16.5	7.45	7.46	-0.1
1900	21.5	4.24	4.18	+1.4
1900	26.5	2.71	2.91	-7.9
1900	31.5	1.77	1.75	+1.1

Table 4. Sphere phantom: Comparison of the measured and FDTD-calculated peak 1-g SARs for three spacings each at 840 and 1900 MHz, radiated power normalized to 0.5 W.

Frequency (MHz)	Distance (mm) Between $\lambda/2$ Dipole and the Box	SAR (W/kg)		Difference (%)
		Measured	FDTD	
840	5	6.78	6.77	+0.23
840	15	3.41	3.27	+4.22
840	25	1.85	1.68	+9.51
1900	5	17.45	18.01	-3.21
1900	15	4.96	5.05	-1.81
1900	25	1.69	1.77	-4.73

Table 5. **The SARs measured for the Fujitsu Model EC2500 Cellular Telephone normalized to a maximum planned power of 28.0 dBm (631 mW) at the low-end frequency of 824.70 MHz. Antenna left retracted.** The SARs in W/kg are measured with a step size of 2 mm for the highest SAR region of the model.

1-g SAR = 0.947 W/kg

a. At depth of 1 mm

1.204	1.268	1.258	1.205	1.184
1.235	1.270	1.258	1.218	1.178
1.223	1.263	1.243	1.220	1.178
1.217	1.223	1.200	1.188	1.146
1.167	1.170	1.162	1.142	1.104

b. At depth of 3 mm

1.051	1.101	1.096	1.057	1.041
1.076	1.105	1.097	1.067	1.035
1.070	1.102	1.088	1.071	1.038
1.068	1.078	1.058	1.049	1.016
1.038	1.039	1.034	1.017	0.983

c. At depth of 5 mm

0.917	0.956	0.955	0.926	0.915
0.937	0.961	0.956	0.934	0.909
0.937	0.961	0.952	0.939	0.913
0.937	0.948	0.932	0.925	0.900
0.921	0.922	0.919	0.904	0.874

d. At depth of 7 mm

0.803	0.833	0.834	0.813	0.806
0.818	0.838	0.835	0.819	0.801
0.821	0.840	0.834	0.824	0.805
0.824	0.835	0.822	0.816	0.798
0.818	0.818	0.816	0.804	0.778

e. At depth of 9 mm

0.708	0.731	0.734	0.719	0.714
0.720	0.735	0.734	0.722	0.709
0.724	0.739	0.735	0.727	0.713
0.727	0.737	0.727	0.723	0.709
0.727	0.727	0.725	0.715	0.694

Table 6. **The SARs measured for the Fujitsu Model EC2500 Cellular Telephone normalized to a maximum planned power of 28.0 dBm (631 mW) at the low-end frequency of 824.70 MHz. Antenna pulled out.** The SARs in W/kg are measured with a step size of 2 mm for the highest SAR region of the model.

1-g SAR = 0.984 W/kg

a. At depth of 1 mm

1.228	1.301	1.304	1.258	1.243
1.253	1.300	1.299	1.277	1.244
1.250	1.295	1.290	1.270	1.237
1.232	1.261	1.252	1.246	1.212
1.195	1.207	1.210	1.197	1.161

b. At depth of 3 mm

1.070	1.130	1.135	1.103	1.093
1.090	1.129	1.131	1.117	1.092
1.093	1.130	1.127	1.114	1.090
1.086	1.109	1.102	1.099	1.073
1.064	1.074	1.077	1.067	1.036

c. At depth of 5 mm

0.935	0.982	0.989	0.968	0.962
0.949	0.982	0.986	0.977	0.959
0.956	0.986	0.985	0.979	0.960
0.958	0.976	0.971	0.969	0.950
0.947	0.956	0.959	0.952	0.924

d. At depth of 7 mm

0.820	0.858	0.865	0.852	0.849
0.831	0.858	0.863	0.858	0.846
0.840	0.865	0.864	0.862	0.850
0.848	0.862	0.858	0.858	0.843
0.845	0.852	0.855	0.850	0.827

e. At depth of 9 mm

0.728	0.758	0.765	0.756	0.756
0.735	0.758	0.763	0.760	0.752
0.744	0.765	0.765	0.765	0.757
0.755	0.767	0.764	0.764	0.754
0.757	0.763	0.766	0.761	0.744

Table 7. **The SARs measured for the Fujitsu Model EC2500 Cellular Telephone normalized to a maximum planned power of 28.0 dBm (631 mW) at the midband frequency of 836.49 MHz. Antenna left retracted.** The SARs in W/kg are measured with a step size of 2 mm for the highest SAR region of the model.

1-g SAR = 0.833 W/kg

a. At depth of 1 mm

1.064	1.123	1.113	1.071	1.045
1.087	1.118	1.113	1.079	1.043
1.077	1.116	1.099	1.077	1.039
1.061	1.077	1.058	1.043	1.013
1.028	1.030	1.021	1.002	0.968

b. At depth of 3 mm

0.929	0.974	0.968	0.936	0.918
0.947	0.971	0.968	0.943	0.915
0.944	0.972	0.960	0.942	0.913
0.934	0.947	0.932	0.921	0.895
0.914	0.914	0.907	0.891	0.860

c. At depth of 5 mm

0.810	0.844	0.842	0.818	0.805
0.824	0.843	0.842	0.823	0.802
0.826	0.846	0.838	0.824	0.802
0.821	0.831	0.819	0.811	0.789
0.810	0.810	0.804	0.791	0.763

d. At depth of 7 mm

0.708	0.734	0.735	0.717	0.709
0.719	0.734	0.733	0.721	0.704
0.723	0.738	0.732	0.721	0.705
0.722	0.730	0.721	0.715	0.697
0.718	0.717	0.712	0.702	0.677

e. At depth of 9 mm

0.623	0.643	0.645	0.632	0.627
0.631	0.643	0.643	0.635	0.623
0.636	0.647	0.643	0.634	0.623
0.637	0.644	0.637	0.632	0.619
0.637	0.636	0.632	0.624	0.604

Table 8. **The SARs measured for the Fujitsu Model EC2500 Cellular Telephone normalized to a maximum planned power of 28.0 dBm (631 mW) at the midband frequency of 836.49 MHz. Antenna pulled out.** The SARs in W/kg are measured with a step size of 2 mm for the highest SAR region of the model.

1-g SAR = 0.885 W/kg

a. At depth of 1 mm

1.107	1.176	1.180	1.136	1.129
1.135	1.179	1.174	1.153	1.116
1.125	1.168	1.163	1.151	1.121
1.111	1.133	1.124	1.123	1.093
1.081	1.087	1.089	1.077	1.045

b. At depth of 3 mm

0.963	1.018	1.025	0.995	0.989
0.986	1.021	1.021	1.005	0.980
0.982	1.017	1.014	1.006	0.983
0.977	0.996	0.990	0.989	0.965
0.960	0.967	0.969	0.960	0.932

c. At depth of 5 mm

0.840	0.883	0.892	0.872	0.867
0.857	0.885	0.887	0.877	0.861
0.858	0.886	0.885	0.880	0.864
0.859	0.876	0.872	0.871	0.853
0.852	0.860	0.862	0.855	0.831

d. At depth of 7 mm

0.736	0.769	0.778	0.767	0.764
0.748	0.771	0.775	0.769	0.759
0.752	0.775	0.775	0.772	0.762
0.759	0.773	0.770	0.770	0.756
0.758	0.766	0.767	0.762	0.742

e. At depth of 9 mm

0.651	0.677	0.686	0.679	0.678
0.660	0.678	0.683	0.679	0.674
0.665	0.684	0.684	0.683	0.677
0.674	0.686	0.684	0.684	0.674
0.677	0.684	0.685	0.682	0.667

Table 9. **The SARs measured for the Fujitsu Model EC2500 Cellular Telephone normalized to a maximum planned power of 28.0 dBm (631 mW) at the high end frequency of 848.97 MHz. Antenna left retracted.** The SARs in W/kg are measured with a step size of 2 mm for the highest SAR region of the model.

1-g SAR = 0.761 W/kg

a. At depth of 1 mm

0.973	1.022	1.017	0.977	0.959
0.996	1.023	1.014	0.989	0.958
0.990	1.020	1.006	0.985	0.953
0.974	0.987	0.971	0.962	0.928
0.946	0.948	0.942	0.924	0.893

b. At depth of 3 mm

0.846	0.885	0.882	0.853	0.839
0.865	0.887	0.882	0.852	0.838
0.865	0.888	0.877	0.861	0.835
0.857	0.867	0.855	0.845	0.818
0.840	0.840	0.835	0.821	0.792

c. At depth of 5 mm

0.735	0.766	0.765	0.744	0.734
0.750	0.769	0.765	0.751	0.732
0.755	0.772	0.764	0.752	0.731
0.752	0.760	0.751	0.742	0.721
0.744	0.743	0.739	0.728	0.702

d. At depth of 7 mm

0.640	0.664	0.665	0.651	0.644
0.652	0.667	0.666	0.656	0.642
0.659	0.673	0.667	0.657	0.641
0.661	0.667	0.659	0.652	0.636
0.658	0.657	0.653	0.644	0.622

e. At depth of 9 mm

0.562	0.581	0.582	0.573	0.568
0.571	0.583	0.583	0.575	0.566
0.579	0.589	0.584	0.577	0.565
0.582	0.586	0.580	0.574	0.563
0.582	0.581	0.578	0.570	0.553

Table 10. **The SARs measured for the Fujitsu Model EC2500 Cellular Telephone normalized to a maximum planned power of 28.0 dBm (631 mW) at the high end frequency of 848.97 MHz. Antenna pulled out.** The SARs in W/kg are measured with a step size of 2 mm for the highest SAR region of the model.

1-g SAR = 0.888 W/kg

a. At depth of 1 mm

1.113	1.183	1.188	1.151	1.135
1.141	1.187	1.186	1.161	1.132
1.136	1.180	1.173	1.159	1.132
1.119	1.148	1.133	1.126	1.099
1.086	1.093	1.092	1.084	1.053

b. At depth of 3 mm

0.966	1.023	1.030	1.002	0.992
0.990	1.026	1.028	1.010	0.988
0.990	1.026	1.022	1.011	0.989
0.984	1.006	0.995	0.991	0.969
0.964	0.971	0.971	0.964	0.937

c. At depth of 5 mm

0.840	0.886	0.893	0.873	0.868
0.859	0.887	0.890	0.879	0.863
0.863	0.892	0.890	0.883	0.865
0.866	0.882	0.874	0.872	0.854
0.856	0.862	0.862	0.857	0.833

d. At depth of 7 mm

0.733	0.769	0.777	0.763	0.762
0.748	0.771	0.774	0.768	0.757
0.755	0.777	0.777	0.773	0.759
0.762	0.774	0.770	0.769	0.755
0.760	0.766	0.766	0.762	0.743

e. At depth of 9 mm

0.646	0.675	0.683	0.673	0.674
0.658	0.676	0.680	0.676	0.670
0.666	0.683	0.684	0.681	0.672
0.675	0.684	0.682	0.682	0.671
0.677	0.682	0.683	0.680	0.664

Table 11. Summary of the measured peak 1-g SARs for the Fujitsu Model EC2500 Cellular Telephone for a maximum planned power of 28.0 dBm (631 mW).

Frequency MHz	1-g SAR (W/kg)	
	Antenna Retracted	Antenna Pulled Out
824.70	0.947	0.984
836.49	0.833	0.885
848.97	0.761	0.888

Fig. 1. The Fujitsu Cellular Telephone.

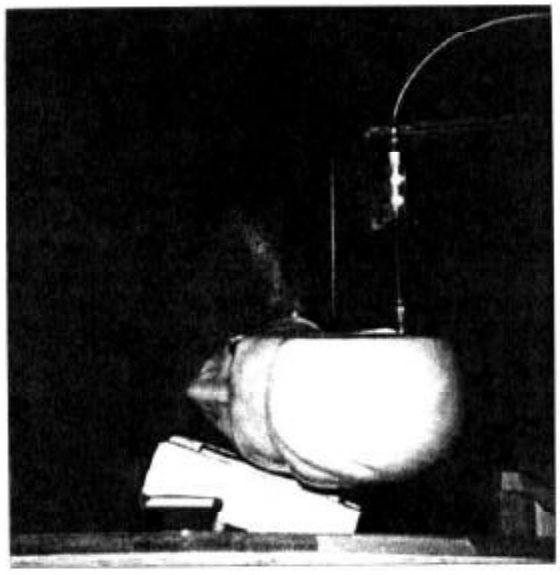

Fig. 2. The phantom model used for measurement of the SAR distribution for Fujitsu Model EC2500 Cellular Telephone.

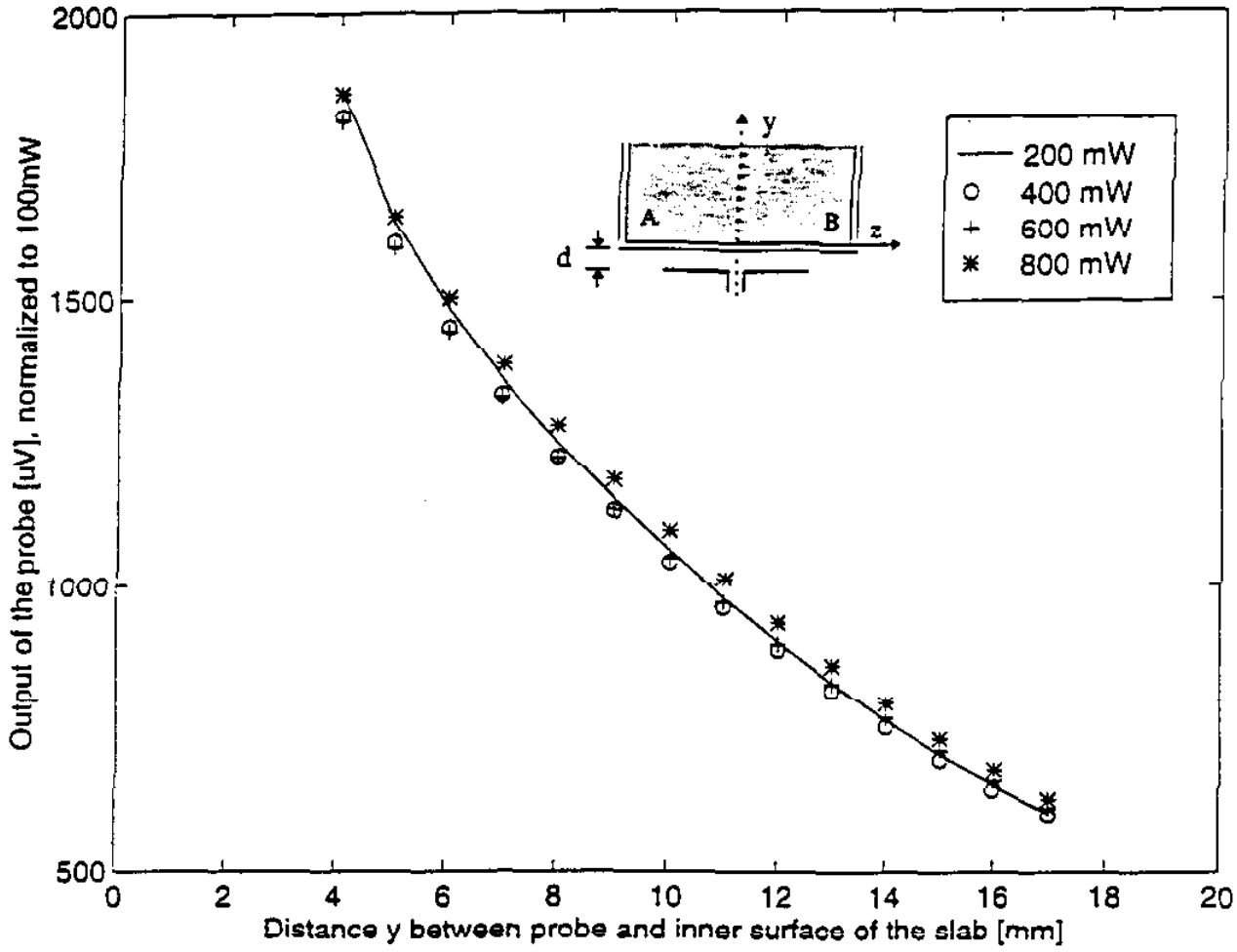

Fig. 3a. Test for square-law behavior at 840 MHz: Variation of the output voltage (proportional to $|E_i|^2$) for different radiated powers normalized to 0.1 W.

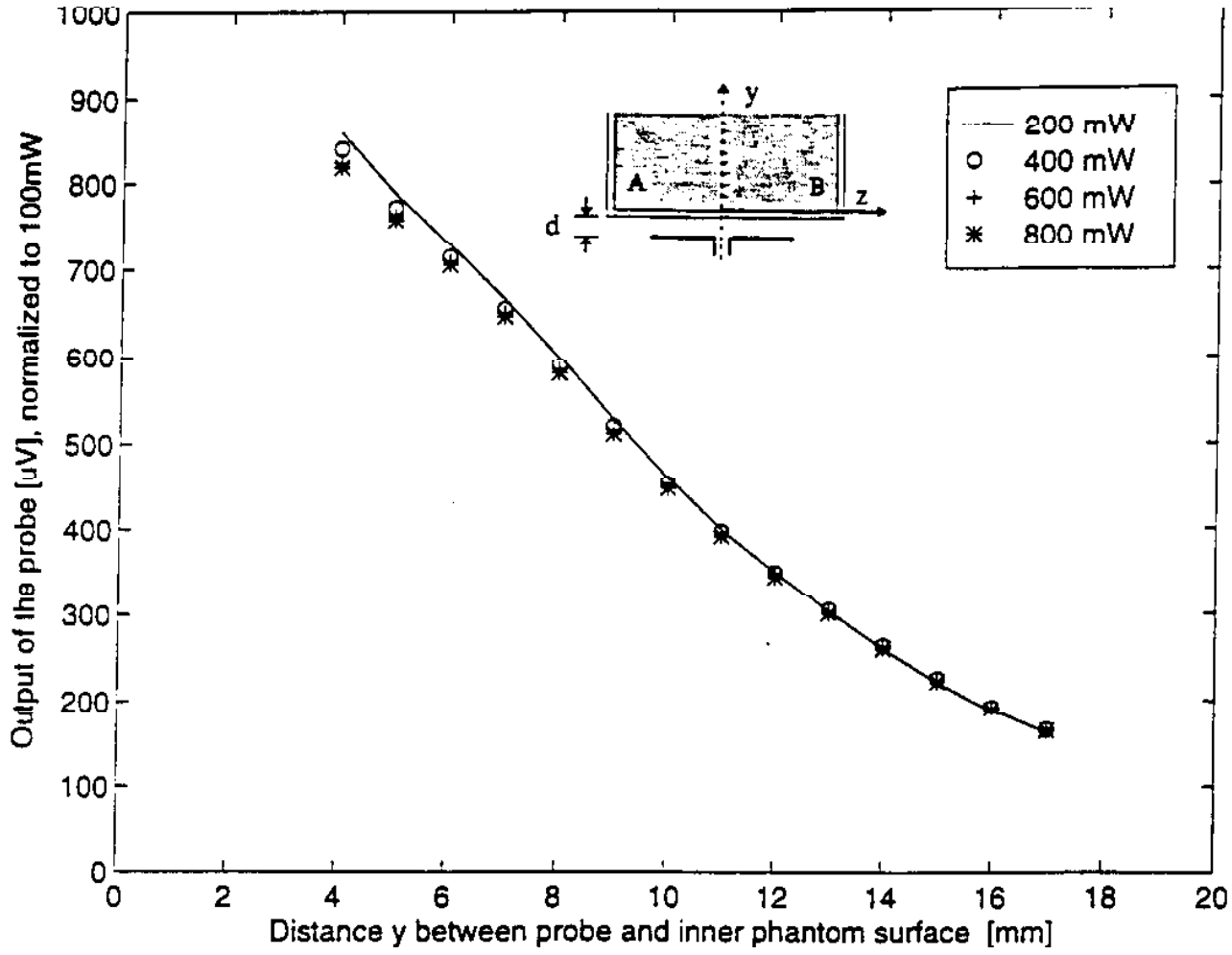

Fig 3b. Test for square-law behavior at 1900 MHz: Variation of the output voltage (proportional to $|E_i|^2$) for different radiated powers normalized to 0.1 W.

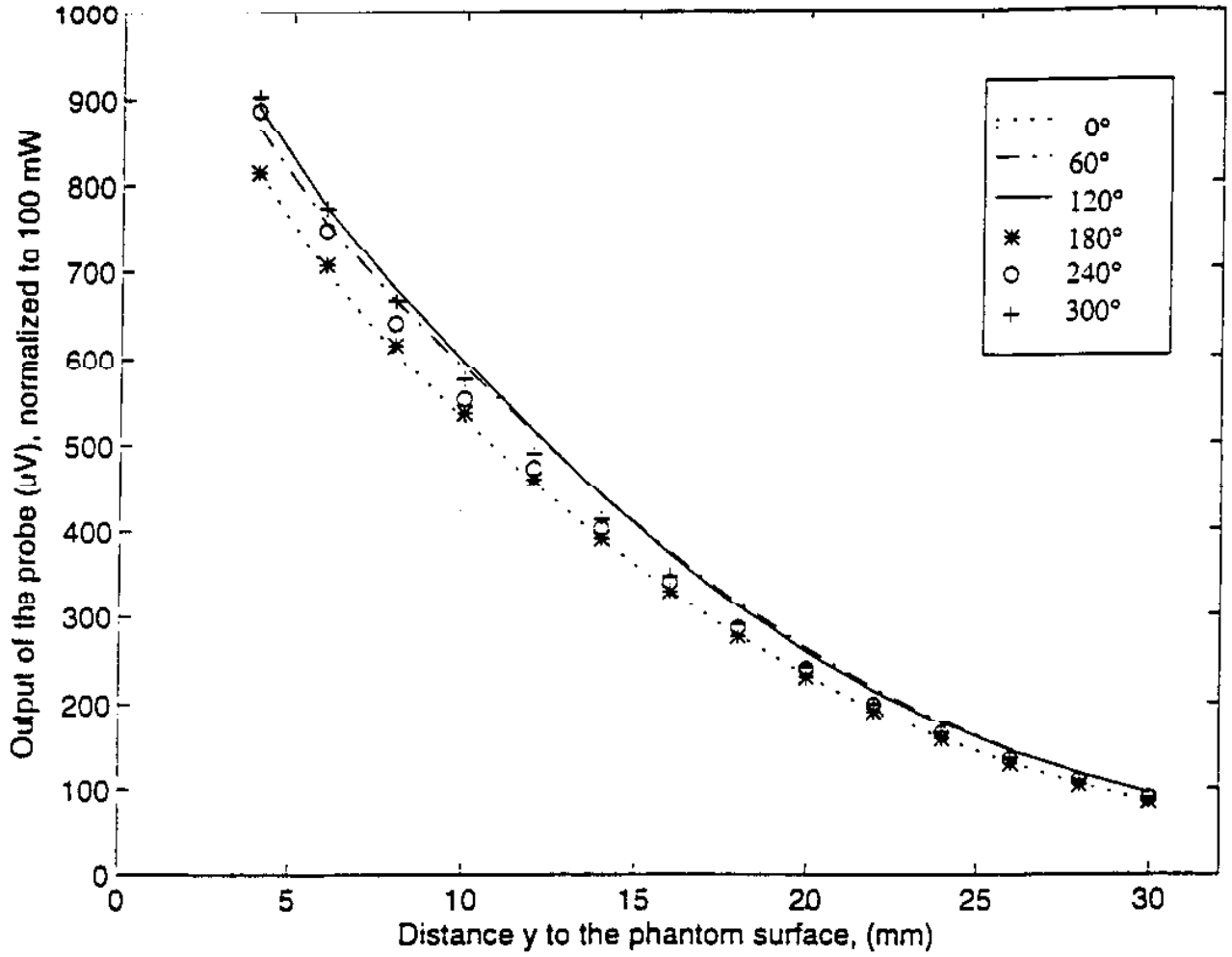

Fig. 4a Test for isotropy: The model shown in Fig. 2 was used with nominal half wavelength dipole radiator of length 178 mm at 840 MHz.

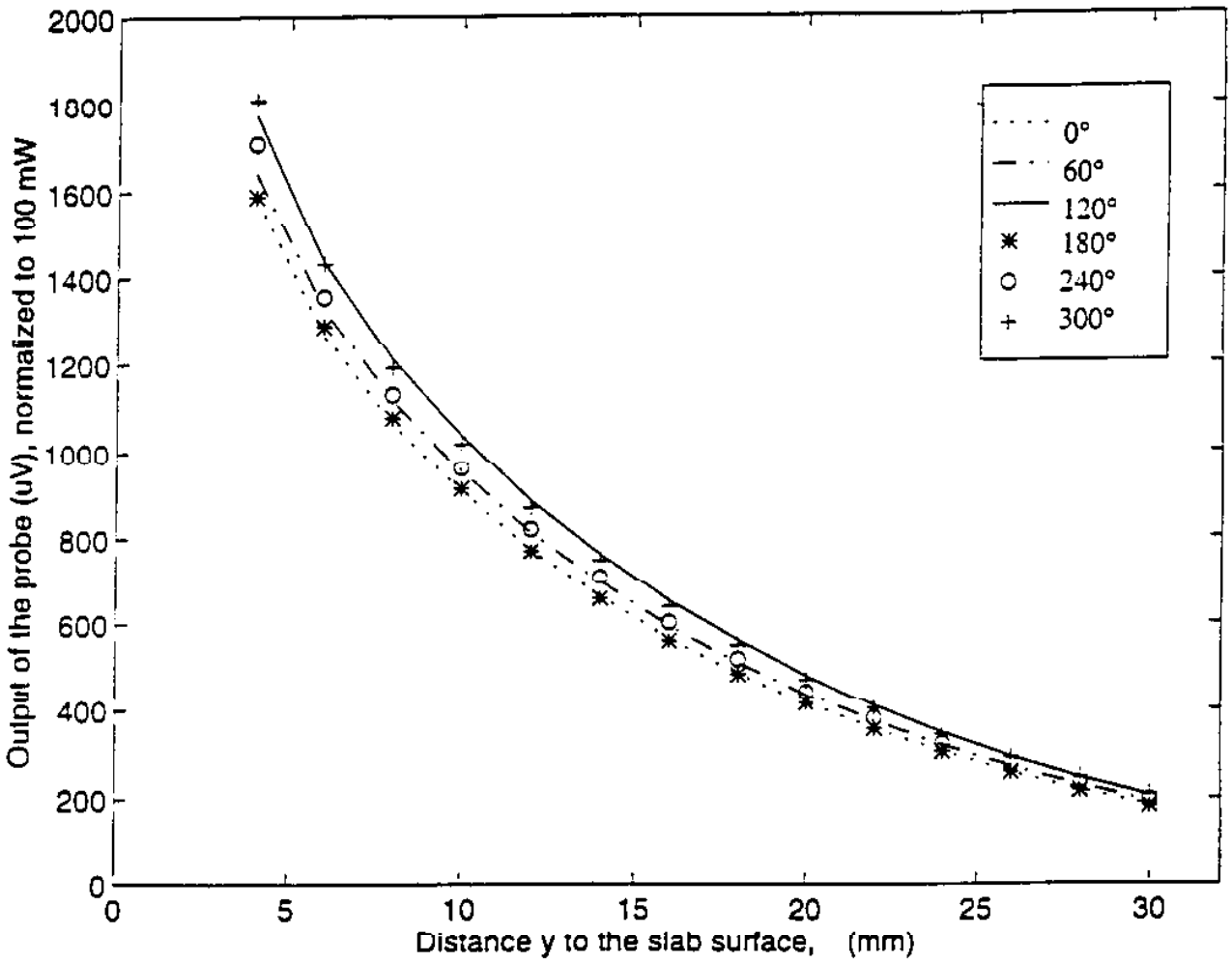

Fig 4b. Test for isotropy: The model shown in Fig. 2 was used with nominal half wavelength dipole radiator of length 77 mm at 1900 MHz.

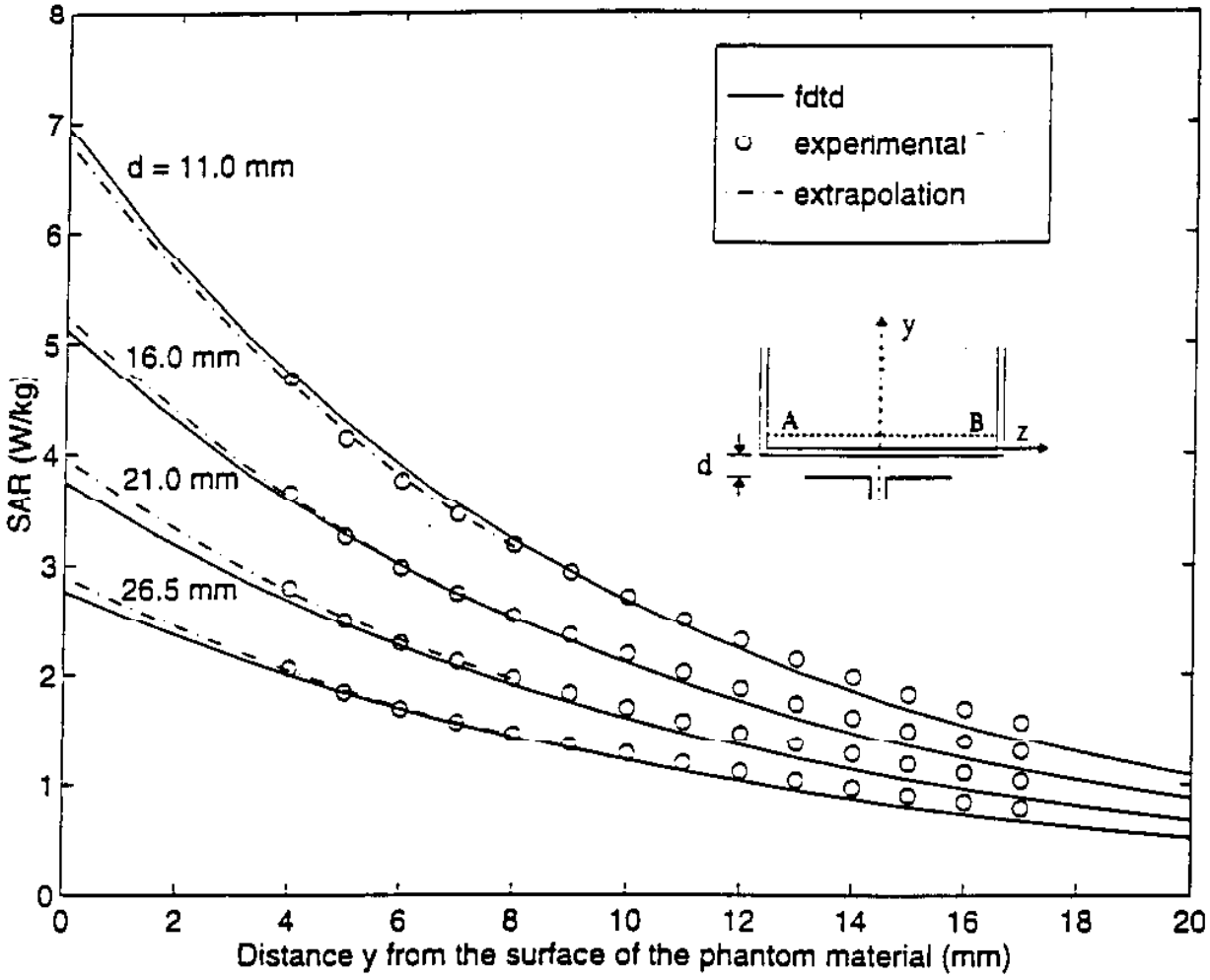

Fig. 5a. Comparison of the calculated and measured SAR variations for a box phantom of dimensions 30 × 15 × 50 cm; 840 MHz; λ/2 dipole antenna; 0.5 W radiated power. Calibration factor for the Narda Model 8021 probe at 840 MHz = 0.49 (mW/kg)/μV. Measured for the phantom material $\varepsilon_r = 41.1$, $\sigma = 1.06$ S/m.

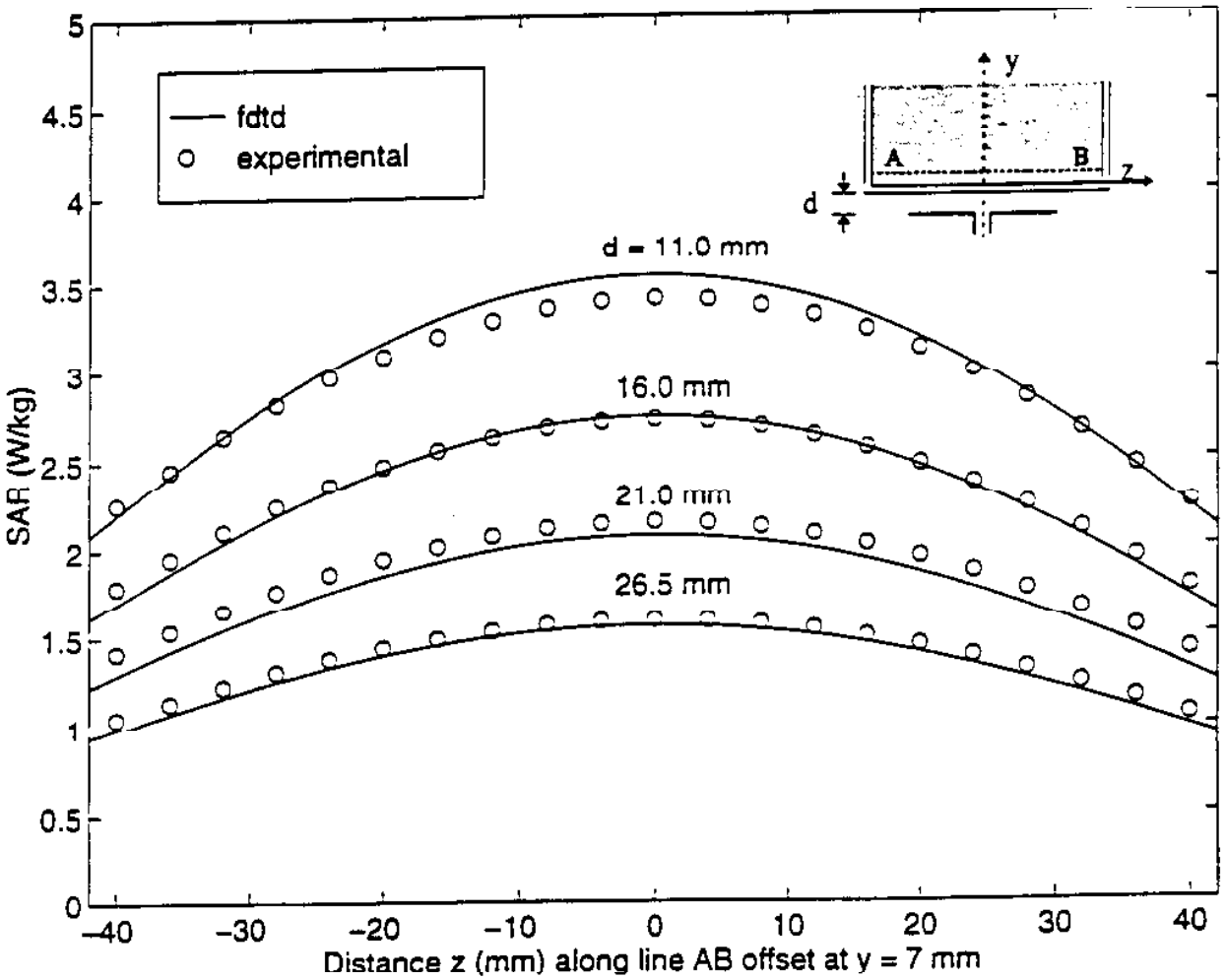

Fig. 5b. Comparison of the calculated and measured SAR variations for a box phantom of dimensions 30 × 15 × 50 cm for a line AB parallel to the z axis at a distance y = 7 mm from the surface of the phantom material: 840 MHz; λ/2 dipole antenna; 0.5 W radiated power. Calibration factor for the Narda Model 8021 probe at 840 MHz = 0.49 (mW/kg)/μV. Measured for the phantom material $\varepsilon_r = 41.1$, $\sigma = 1.06$ S/m.

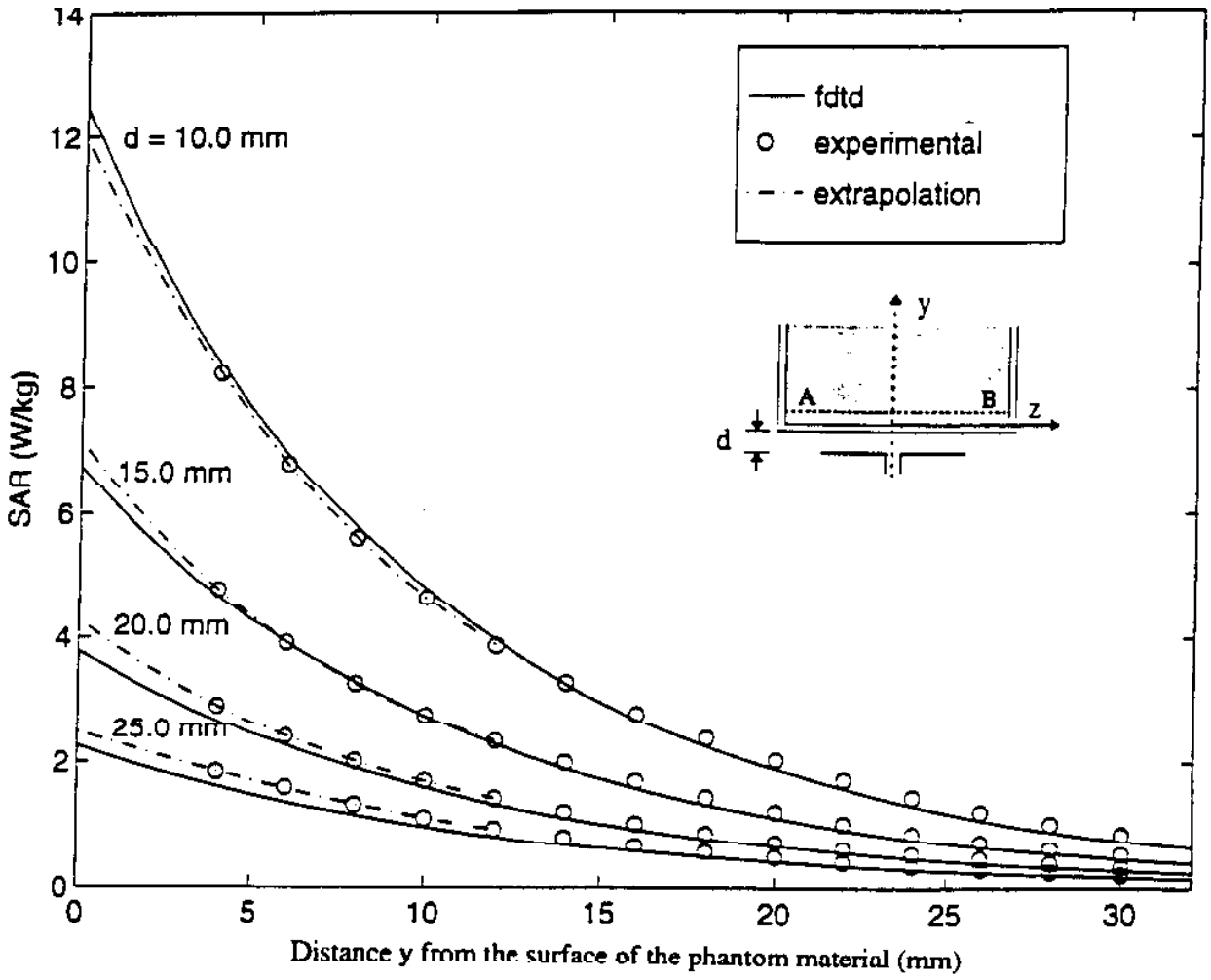

Fig. 6a. Comparison of the calculated and measured SAR variations for a box phantom of dimensions 30 × 15 × 50 cm; 1900 MHz; λ/2 dipole antenna; 0.5 W radiated power. Calibration factor for the Narda Model 8021 probe at 1900 MHz = 0.84 (mW/kg)/μV. Measured for the phantom material $\varepsilon_r = 45.5$, $\sigma = 1.31$ S/m.

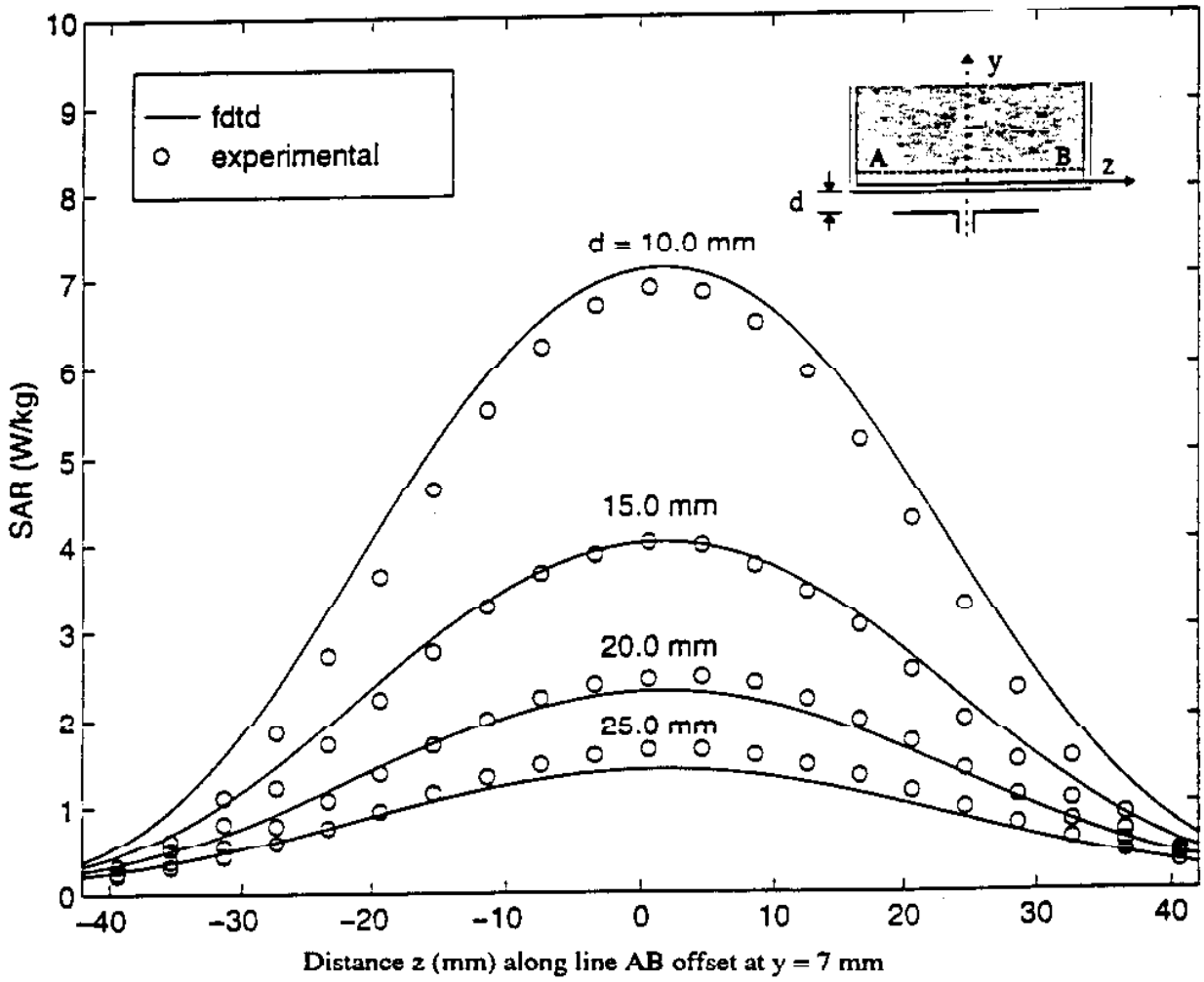

Fig. 6b. Comparison of the calculated and measured SAR variations for a box phantom of dimensions 30 × 15 × 50 cm for a line AB parallel to the z axis at a distance y = 7 mm from the surface of the phantom material; 1900 MHz; λ/2 dipole antenna; 0.5 W radiated power. Calibration factor for the Narda Model 8021 probe at 1900 MHz = 0.84 (mW/kg)/μV. Measured for the phantom material ε_r = 45.5, σ = 1.31 S/m.

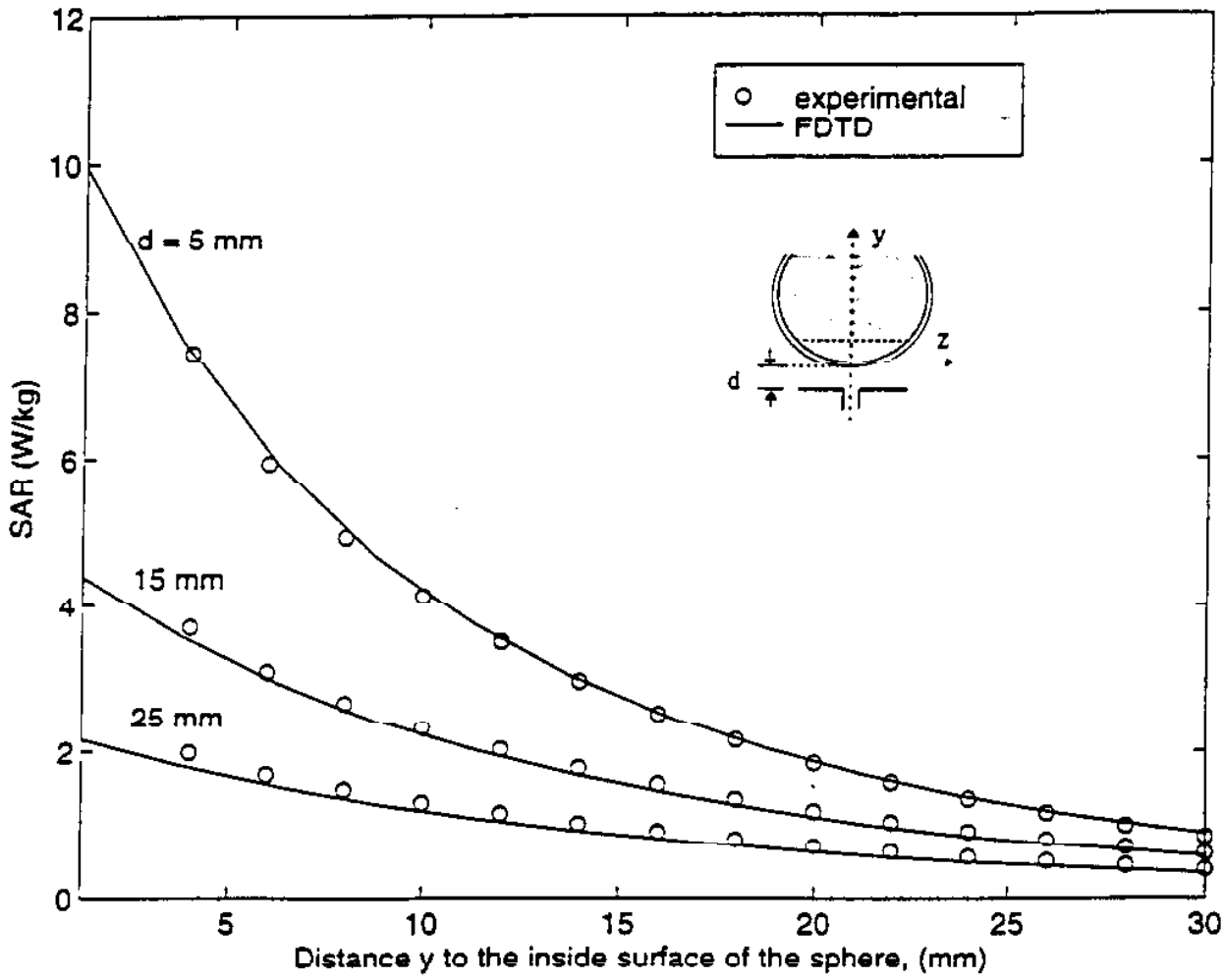

Fig. 7a. Comparison of measured and FDTD-calculated SAR variations at 840 MHz for a glass sphere model of outer diameter 22.3 cm and thickness 5 mm. SARs normalized to a radiated power of 0.5 W. Calibration factor = 0.49 (mW/kg)/μV. Measured for the phantom material $\varepsilon_r = 41.1$. $\sigma = 1.06$ S/m.

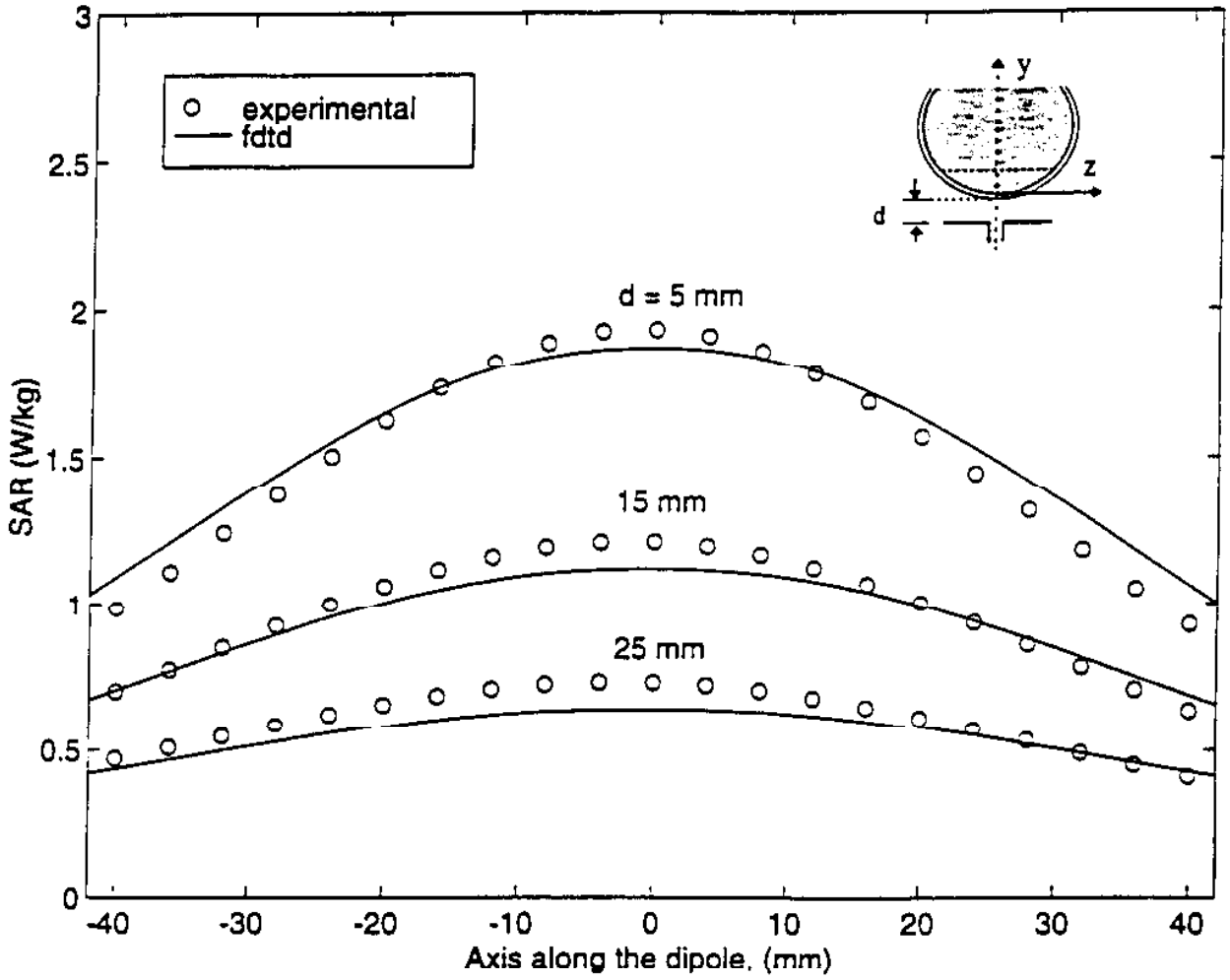

Fig. 7b. Comparison of calculated and measured SAR variations at 840 MHz for a plane at a distance of 20 mm from the lowest point on the inside of the sphere. SARs normalized to a radiated power of 0.5 W. Calibration factor = 0.49 (mW/kg)/μV. Measured for the phantom material $\epsilon_r = 41.1$, $\sigma = 1.06$ S/m.

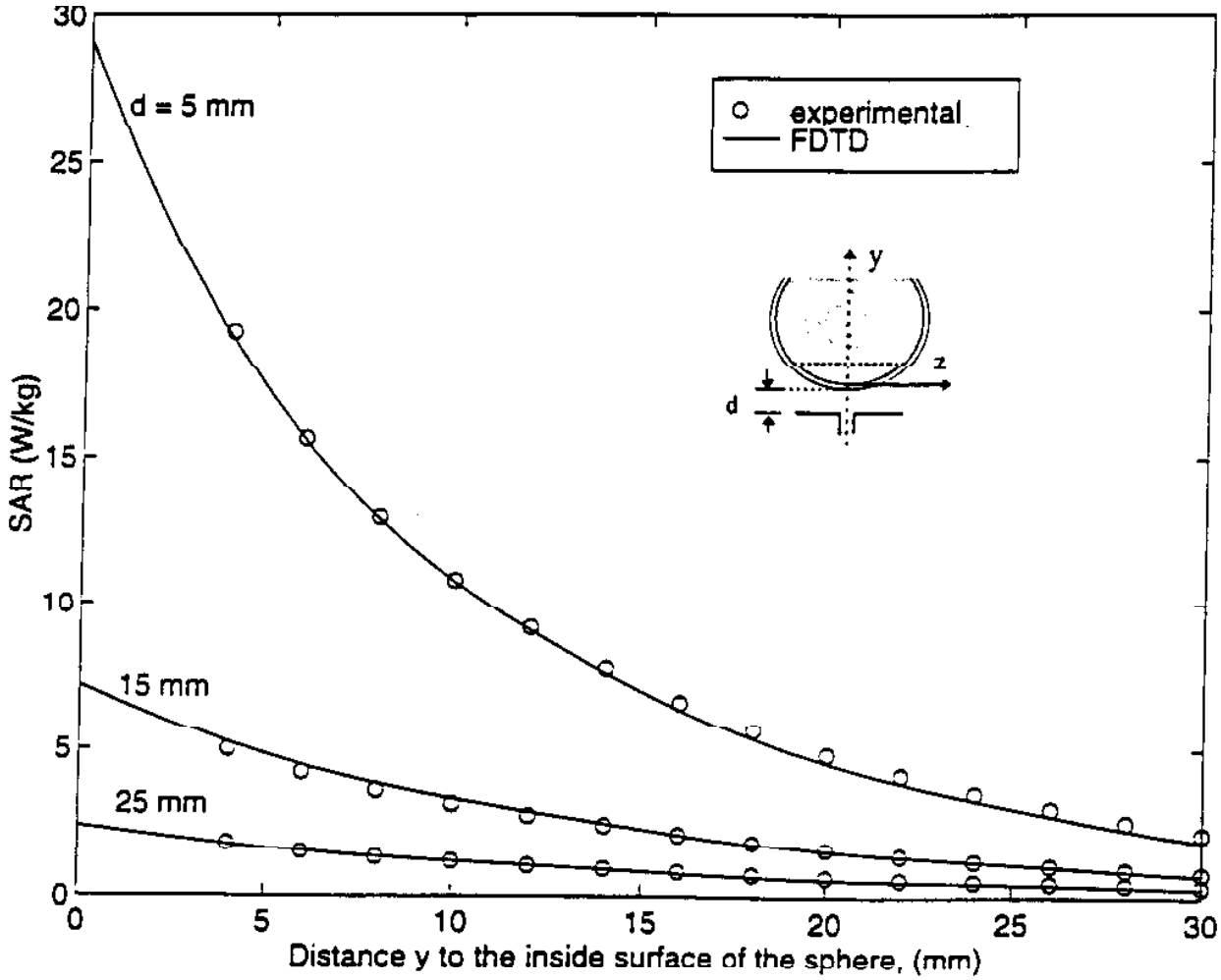

Fig. 8a. Comparison of measured and FDTD-calculated SAR variations at 1900 MHz for a glass sphere model of outer diameter 22.3 cm and thickness 5 mm. SARs normalized to a radiated power of 0.5 W. Calibration factor = 0.84 (mW/kg)/μV. Measured for the phantom material $\varepsilon_r = 45.5$, $\sigma = 1.31$ S/m.

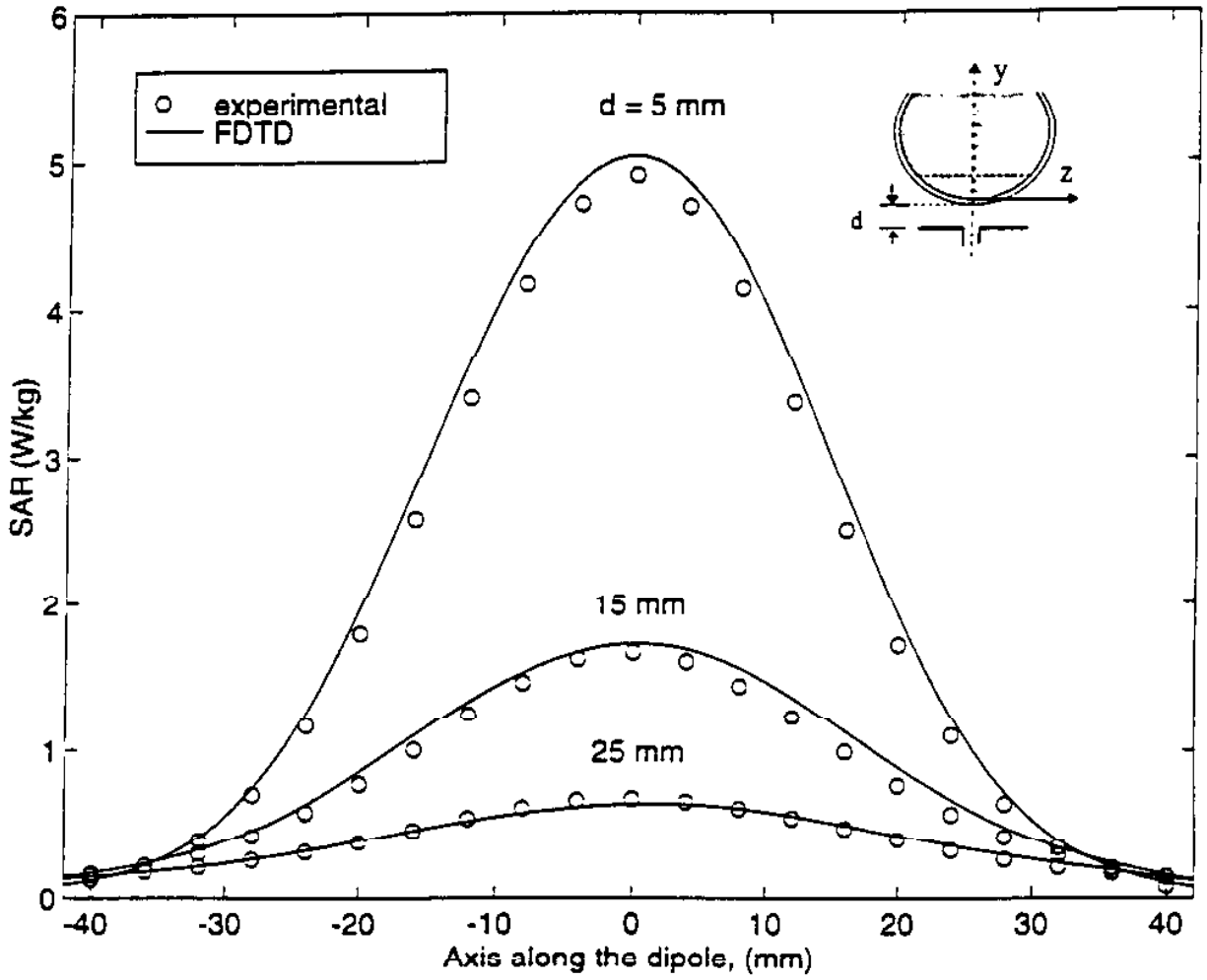

Fig. 8b. Comparison of calculated and measured SAR variations at 1900 MHz for a plane at a distance of 20 mm from the lowest point on the inside of the sphere. SARs normalized to a radiated power of 0.5 W. Calibration factor = 0.84 (mW/kg)/μV. Measured for the phantom material $\varepsilon_r = 45.5$, $\sigma = 1.31$ S/m.